*Progress In Electromagnetics Research, Vol. 116, 457–473, 2011*

# CUDA IMPLEMENTATION IN THE EM SCATTERING OF A THREE-LAYER CANOPY

**W.-Q. Jiang[1], M. Zhang[1, *], H. Chen[1], and Y.-G. Lu[2]**

[1]School of Science, Xidian University, Xi'an 710071, China

[2]Science and Technology on Electromagnetic Scattering Laboratory, Beijing 100854, China

**Abstract**—Calculation of the EM scattered fields from a three-layer canopy faces intensive computational burden, when the area becomes large and obviously lames the application of the traditional serial algorithm. With the development of graphics hardware, the Graphics Processing Unit (GPU) can be used to calculate the electromagnetic (EM) scattering problems parallelly. In this paper, the Compute Unified Device Architecture (CUDA) is combined with the four-path method and the reciprocity theorem to improve the speed of calculating the EM scattering properties from a three layer-canopy which are simulated by employing the Monte-Carlo method. We get a highest speedup of 294 times in comparison with the original serial algorithm on a Core (TM) i5 CPU with a GTS460 GPU as a coprocessor.

## 1. INTRODUCTION

Researchers have been doing a lot of work in the study of the vegetation scattering [1–9] which has an impact on the electromagnetic scattering in forest communication, target recognition, environmental monitoring, and so on. The three-layer canopy comprises of the crown layer, the trunk layer and the underlying surface [10]. Among the three layers, the crown layer is characterized by the average height and diameter of a tree's crown and size, shape, and dielectric constant distributions of the leaves.

*Received 17 March 2011, Accepted 9 May 2011, Scheduled 17 May 2011*

* Corresponding author: Min Zhang (mzhang@mail.xidian.edu.cn).

The four-path approximation, which is widely used to calculate the EM scattering from targets above a surface [11], is employed to calculate the EM scattering of the crown-layer. The leaves in the crown layer are modeled by elliptical discs with random orientations and positions. The EM scattered field from each single leaf is calculated under the generalized Rayleigh-Gans (GRG) approximation [5, 12, 13], and the underlying surface is treated as a flat surface. The EM scattered field from each leaf is the sum EM scattered fields of the four paths.

The reciprocity theorem [14] is introduced to study the problem of EM scattered field from the trunk-layer. The trunk-layer consists of many dielectric cylinders of finite length. The total EM scattered field from the trunk-layer includes the first order scattered field excited by the incidence field and the second order scattered field excited by the first order scattered fields of other cylinders. Therefore, there are $N^2$ fields need to calculate for $N$ trunks.

As the number of scatterers gets large, intensive computational burden occurs and obviously lames the application of the traditional serial algorithm. Nevertheless, with the emergence of CUDA [15, 16], the EM scattered fields from hundreds of scatterers can be calculated synchronously on a PC equipped with the CUDA compatible GPU. And many researchers have implemented the programs on GPU to solve the EM scattering problems and gotten tens of times speedup [17–24]. However, only a few CUDA-based methods have been implemented in vegetation scattering. Here, with a 336 stream processors GPU (GTX460), the CUDA parallel programs can create many threads executing synchronously on the GPU and each thread is able to calculate EM scattered field from its own target. The CUDA parallel algorithm has two parts. The first part deals with the EM scattering properties from the crow-layer which has $M$ leaves. It creates $M$ threads, each of which calculates the EM scattered fields from the $m$th scatterer which is identified by the sequence number $m$th of the thread. And send the result to the main memory after all threads finish their task. The second part deals with the trunk-layer. It creates $N$ threads, each of which calculates the first order field of the trunk. Then, it creates $N*(N-1)$ threads to calculate the second order fields of each two trunks under the reciprocity theorem. For there are hundreds of threads executing at the same time, the CUDA parallel program can calculate hundreds of fields at a time and reduce the calculation time obviously. We obtain a highest speedup of 294 times with a GTX460 GPU as a coprocessor. With the help of CUDA, it is more convenient and faster to calculate the EM scattering properties from the field in large scope.

## 2. EM SCATTERING FROM THE THREE-LAYER CANOPY

### 2.1. Three-layer Canopy Model

The three-layer canopy model is divided into three regions: the crown layer of thickness $d_c$, the trunk layer of thickness $d_t$ and the ground surface, shown in Fig. 1. The ground surface is treated as a flat surface. The trunk layer is comprised of cylinders of radius $a$ and length $l = d_t$. And the cylinders distribute uniformly, in a round area of radius $r_g$, over the ground surface. The crown layer is comprised of leaves which are distributed uniformly, in a round area of radius $r_g$, over the ground surface. The orientations of leaves are simulated by using Monte-Carlo method. The size of leaves which are described as regular ellipsoids satisfies the formula $k_0 c(\sqrt{\varepsilon_r} - 1) \ll 1$, where $k_0$ is the vacuum wave number, $c$ the smallest dimension and $\varepsilon_r$ the scatterer dielectric constant relative to that of the vacuum, in the microwave range. And the EM scattering of the crown layer can be calculated under the GRG approximation [5, 25–28].

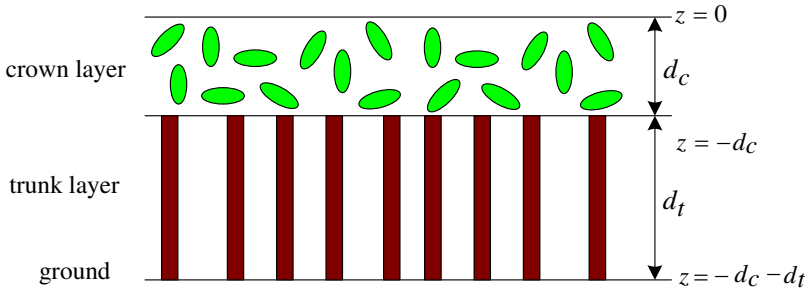


**Figure 1.** Three-layer canopy model.

**Table 1.** Parameters of three-layer canopy.

| Leaf | | Trunk | | Other parameters | | |
|---|---|---|---|---|---|---|
| dielectric constant | (13.6,5.6) | dielectric constant | (17.7,7.5) | Ground | dielectric constant | (17.7,7.5) |
| Length | 6cm | Radius | 5cm | $r_g$ | | 2m |
| Width | 3cm | Height | 118cm | Crown layer thickness | | 0.3m |
| Thickness | 1mm | | | | | |
| Density | 5000/$m^3$ | Density | 1.5/$m^2$ | Trunklayer thickness | | 1.18m |
| PDF | Uniform | PDF | vertical | | | |

As shown in Fig. 1, the parameters of wheat at $L$ band are given in Tab. 1. The distribution of the leaves' positions is uniform, and the orientation probability density function (PDF) of leaves follows Eq. (1).

$$\begin{aligned} p_m(\alpha, \beta, \gamma) &= p_m(\alpha) \cdot p_m(\beta) \cdot p_m(\gamma) \\ p_m(\alpha) &= \frac{1}{2\pi} \\ p_m(\beta) &= \frac{1}{\beta_{2m} - \beta_{1m}}, \quad \beta_{1m} \le \beta \le \beta_{2m} \\ p_m(\gamma) &= \frac{1}{\gamma_{2m} - \gamma_{1m}}, \quad \gamma_{1m} \le \gamma \le \gamma_{2m} \end{aligned} \tag{1}$$

where $\alpha$, $\beta$ and $\gamma$ represent the rotation angles, shown in Fig. 2. The $x$, $y$ and $z$ are the axes of the reference coordinates, and the $x_b$, $y_b$ and $z_b$ represent the axes of the local coordinates of the scatterer. The center point of the leaf is set as the origin of coordinates. And we assume that $\beta_{1m} = 25°$, $\beta_{2m} = 35°$, $\gamma_{1m} = 0°$ and $\gamma_{2m} = 90°$.

## 2.2. EM Scattered Field from Crown Layer

For sparse media like vegetation, Foldy's approximation [29–33] can be employed to account for the absorption and scattering effects introduced by the medium. The propagation of coherent wave with $E_v$ and $E_h$ as the horizontal and vertical components of the electric field is governed by

$$\frac{dE_v}{ds} = (jk_0 + M_{vv})E_v + M_{vh}E_h \tag{2}$$

$$\frac{dE_h}{ds} = (jk_0 + M_{hh})E_h + M_{hv}E_v \tag{3}$$

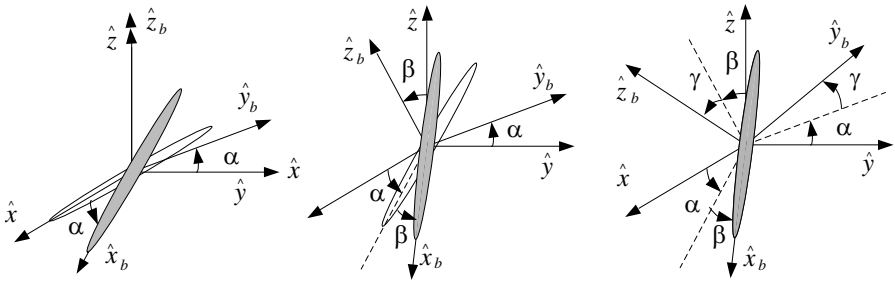


**Figure 2.** The angle $\alpha$, $\beta$ and $\gamma$.

where $s$ is the distance along the direction of propagation, and

$$M_{pq} = \frac{j2\pi\, n_0}{k_0}\langle F_{pq}(\theta,\phi;\theta,\phi\ )\rangle, \qquad p,q = v,h \tag{4}$$

where $(\theta, \phi)$ defines the direction of propagation, $F_{pq}(\theta, \phi; \theta, \phi)$ is the scattering amplitude tensor [5], $n_0$ is the number density of the scatterers, and $\langle\rangle$ denotes ensemble average over the orientation distribution of the scatterers. For vegetation canopy that exhibits azimuthal symmetry, there is no coupling between the horizontal and vertical components of the coherent field. Hence the cross-polarized components $M_{hv}$, and $M_{vh}$ are zero. The effective propagation constants are given by

$$k_{eq} = k_0 + \frac{M_{qq}}{i} \qquad q = v,h \tag{5}$$

The EM scattered field from the crown-layer is written as

$$E^s_{cp}(\vec{r}) = \sum_{m=1}^{M} \hat{p}_s \cdot \vec{E}^{\,s}_m(\vec{r}, \vec{r}_m) \tag{6}$$

where $M$ is the number of leaves in the crown layer, $\vec{r}_m$ is the position of the $m$th leaf, $\vec{E}^{\,s}_m(\vec{r}, \vec{r}_m)$ is the EM scattered field of the $m$th leaf, and $p$ is the polarization vector. According to the Eq. (6), the CUDA parallel program need to create $M$ threads and the $m$th thread deals with the EM scattered field from the $m$th leaf. Under the application of four-path method, the incident wave may be reflected from a leaf via four main mechanisms, see Fig. 3, and $\vec{E}^{\,s}_m(\vec{r}, \vec{r}_m)$ reduces to

$$\vec{E}^{\,s}_m(\vec{r}, \vec{r}_m) = \vec{E}_{m1} + \vec{E}_{m2} + \vec{E}_{m3} + \vec{E}_{m4} \tag{7}$$

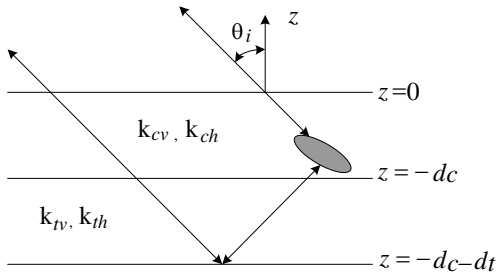


**Figure 3.** EM scattering path of leaves in crown layer.

$$\begin{aligned}
\vec{E}_{m1} &= \bar{\bar{F}}_m(\theta_s, \varphi_s; \theta_i, \varphi_i) \cdot \hat{q}_i \exp(j\varphi_1) \\
\vec{E}_{m2} &= \bar{\bar{F}}_m(\theta_s, \varphi_s; \pi - \theta_i, \varphi_i) \cdot R_q(\theta_i)\hat{q}_i \exp(j\varphi_2) \\
\vec{E}_{m3} &= R_p(\theta_s)\bar{\bar{F}}_m(\pi - \theta_s, \varphi_s; \theta_i, \varphi_i) \cdot \hat{q}_i \exp(j\varphi_3) \\
\vec{E}_{m4} &= R_p(\theta_s)\bar{\bar{F}}_m(\pi - \theta_s, \varphi_s; \pi - \theta_i, \varphi_i) \cdot R_q(\theta_i)\hat{q}_i \exp(j\varphi_4)
\end{aligned} \tag{8}$$

where $\bar{\bar{F}}_m$ is the scattering amplitude tensor of the $m$th leaf, $R$ represents the Fresnel reflectivity of the ground, $p$ and $q$ are the polarization vector, $(\theta_i, \varphi_i)$ define the orientation of the incident wave, and $(\theta_s, \varphi_s)$ define the orientation of the scattering wave. The quantities $\varphi_1$, $\varphi_2$, $\varphi_3$ and $\varphi_4$ represent the phases of the four paths respectively.

### 2.3. EM Scattered Field From Trunk Layer and Total Scattering Coefficient

There are $N$ trunks in the trunk layer. And the EM scattered field is written as

$$E_{tp}^s(\vec{r}) = \sum_{n=1}^{N} \hat{p}_s \cdot \vec{E}_n^s(\vec{r}, \vec{r}_n) \exp(j\Phi) \tag{9}$$

where $\vec{r}_n = x_n\hat{x} + y_n\hat{y} - (d_c + d_t/2)\hat{z}$ is the position of the $n$th trunk. In the backscattering direction, the phase $\Phi$ is written as

$$\Phi = k_0\left[\hat{k}_i(\theta_i, \varphi_i) - \hat{k}_s(\theta_i, \pi + \varphi_i)\right] \cdot \vec{r}_n + 2k_0(\delta_c + d_t)\cos\theta_i + j\frac{2d_c k_{ep}^c + 2d_t k_{ep}^t}{\cos\theta_i} \tag{10}$$

where $k_{ep}^c$ and $k_{ep}^t$ are the effective propagation constants [30] and $\vec{E}_n^s(\vec{r}, \vec{r}_n)$ is the scattered field of the $n$th trunk, including its first order scattered field and the $N-1$ second order scattered fields with other trunks (see Eq. (11))

$$\vec{E}_n^s(\vec{r}, \vec{r}_n) = \vec{E}_n^{s1}(\vec{r}, \vec{r}_n) + \sum_{i=1, i\neq n}^{N} \vec{E}_{ni}^{s2}(\vec{r}, \vec{r}_n, \vec{r}_i) \tag{11}$$

If the trunk of radius $a$ and length $l$ satisfies $k_0 l \gg 1$ and $a/l \ll 1$, the inner field of the cylinder of finite length is estimated by the corresponding field for the same cylinder of infinite length. The first order scattered field can be written as

$$\vec{E}_n^{s1}(\vec{r}, \vec{r}_n) = \frac{e^{jk_0 r}}{r}\frac{k_0^2}{4\pi}\left(\bar{\bar{I}} - \hat{k}_s\hat{k}_s\right)\int_V (\varepsilon_r - 1)\vec{E}_{in}\left(\vec{r}'\right) e^{-jk_0\hat{k}_s\cdot\vec{r}'} d\vec{r}' \tag{12}$$

where $\vec{E}_{in}(\vec{r}')$ is the field inside the cylinder.

By employing the reciprocity theorem [34], the second order field $\vec{E}^{s2}_{ni}(\vec{r}, \vec{r}_n, \vec{r}_i)$ satisfies

$$\hat{p} \cdot \vec{E}^{s2}_{ni} = \int_{V_i} \vec{J}_i \cdot \vec{E}_{ecn} dv \tag{13}$$

where $\vec{J}_i$ is the current density of the $i$th trunk induced by the incident wave. $\vec{E}_{ecn}$ is the scattered field from the $n$th cylinder when illuminated by the radiated field of the elementary current source $\vec{J}_e = \hat{p}\delta(\vec{r} - \vec{r}_0)$ in the far zone. It can be written as

$$\begin{aligned} \vec{E}_{ecn}(\vec{r}) &= \sum_{i=1, i\neq n}^{N} \frac{-jk_0 Z_0}{4\pi r_0} e^{jk_0 r_0} e^{-jk_0 \hat{k}_s \cdot \vec{r}_n} \\ &\quad \vec{F}\left(\varphi_i' - \varphi\right) \cdot H_0^{(1)}\left(k_0 \sin\theta_s \rho_i'\right) e^{-jk_0 \cos\theta_s z_i'} \end{aligned} \tag{14}$$

$$\vec{F}(\varphi_i' - \varphi_s) = \frac{-1}{\sin^2\theta_s} \sum_{m=-\infty}^{\infty} \left[A_m^s \left(\hat{k}_i' \times \hat{k}_i' \times \hat{z}\right) + B_m^s \left(\hat{k}_i' \times \hat{z}\right)\right] e^{jm\left(\varphi_i' - \varphi_s\right)} \tag{15}$$

$$A_m^s = -C_m^{\mathrm{TM}} \hat{k}_s \times \left(\hat{k}_s \times \hat{p}\right) \cdot \hat{z} - j\bar{C}_m \left(\hat{k}_s \times \hat{p}\right) \cdot \hat{z} \tag{16}$$

$$B_m^s = -C_m^{\mathrm{TE}} \left(\hat{k}_s \times \hat{p}\right) \cdot \hat{z} + j\bar{C}_m \hat{k}_s \times \left(\hat{k}_s \times \hat{p}\right) \cdot \hat{z} \tag{17}$$

The expressions $C_m^{\mathrm{TM}}$, $C_m^{\mathrm{TE}}$ and $\bar{C}_m$ are given in [35], the symbol $r_0$ is the position of the source, the symbol $\hat{k}_i' = \sin\theta_s[\cos\varphi_i'\hat{x} + \sin\varphi_i'\hat{y}] - \cos\theta_s\hat{z}$, and the $(\rho_i', \varphi_i', z_i')$ is the cylindrical coordinate of position vector $r_n$.

Considering the ground is flat, the incident and scattered fields are decomposed into $\vec{E}_{\mathrm{TE}}$ and $\vec{E}_{\mathrm{TM}}$ components and the effect of the ground will then be accounted for by modifying these field components by their appropriate reflection coefficients. Thus, the total EM scattered field is

$$\vec{E}^s_{tp} = \hat{p} \cdot \sum_{n=1}^{N} \vec{E}^s_n \tag{18}$$

$$\vec{E}^s_n = \vec{E}^s_{ntg} + \vec{E}^s_{ngt} + \sum_{i=1, i\neq n}^{N} \left[\vec{E}^s_{nittg} + \vec{E}^s_{nitgt} + \vec{E}^s_{nigtt}\right] \tag{19}$$

The expressions $\vec{E}^s_{ntg}$, $\vec{E}^s_{ngt}$, $\vec{E}^s_{nittg}$, $\vec{E}^s_{nitgt}$ and $\vec{E}^s_{nigtt}$ are given in [14], see Fig. 4. According to Eq. (18), we can let the program create $N$

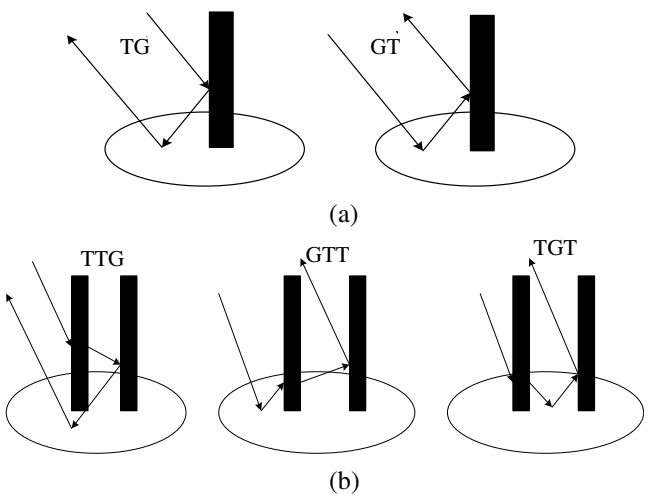


**Figure 4.** EM scattering path of trunks in trunk layer. (a) First order scattering, (b) second order scattering.

threads, and the $n$th thread calculates the first order field of $n$th trunk. For the second order fields, the program can create $N*(N-1)$ threads to deal with the calculation.

According to the Eqs. (6) and (18), the total scattering coefficient $\sigma_{pq}(\vec{k}_s, \vec{k}_i)$ follows

$$\sigma_{pq}\left(\vec{k}_s, \vec{k}_i\right) = \lim_{r\to\infty} \frac{4\pi r^2 \langle |E^s_{cp} + E^s_{tp}|^2 \rangle}{A|E^i_q|^2} \qquad p, q = v, h \qquad (20)$$

where quantity $A$ represents the area of the three-layer canopy, and the symbol $\langle\rangle$ denotes the average over all the realizations.

## 3. SERIAL ALGORITHM AND CUDA PARALLEL ALGORITHM

Figure 5 shows the flow chart of the traditional serial algorithm and the CUDA parallel algorithm. After analysis of the flow chart, we find that the part in the dashed line consumes most of computational complexity. The main difference between the serial algorithm and the CUDA parallel algorithm is how to deal with this part. The serial algorithm program executes on the CPU, and calculates the EM scattered fields from $M$ leaves and $N$ first order fields and $N*(N-1)$ second fields of the $N$ trunks. It calculates the EM scattered fields from the scatterers one by one. Unlike it, the CUDA parallel algorithm

program deals with several hundreds targets at a time in the GPU, see Fig. 6.

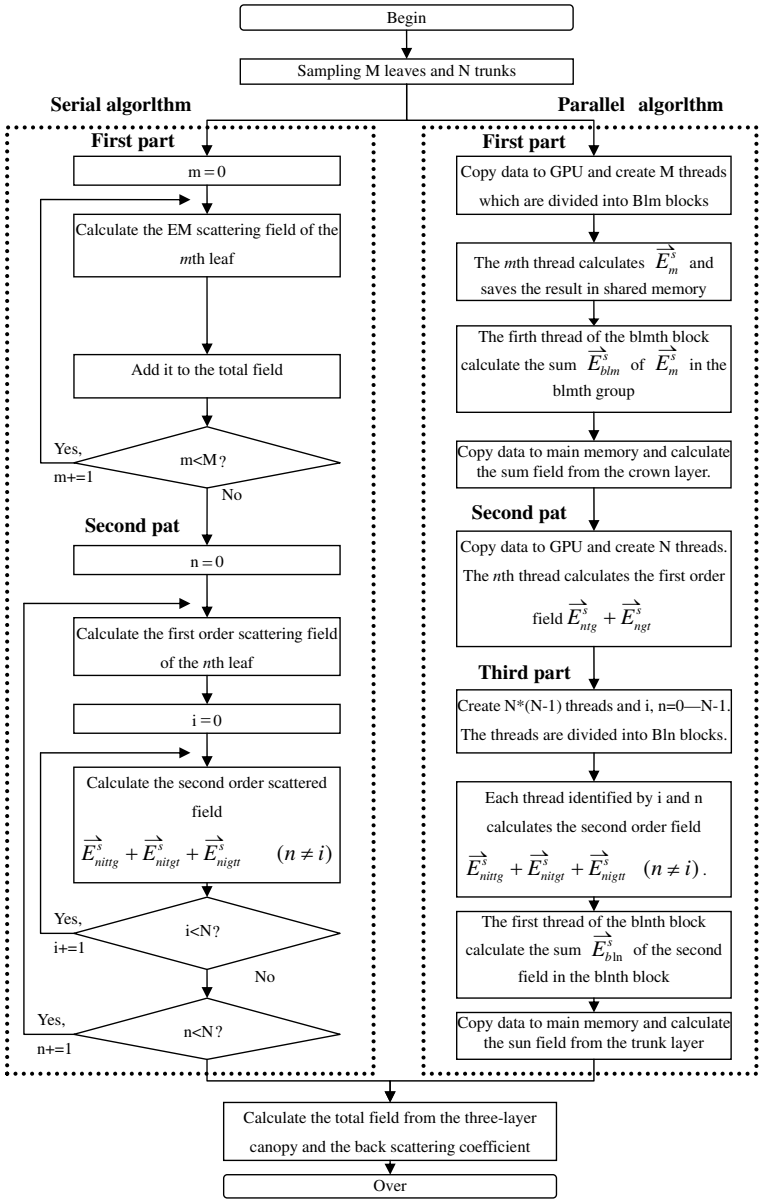


**Figure 5.** Flow chart of serial algorithm and CUDA parallel algorithm.

According to the Eq. (9), Eqs. (18) and (19), the CUDA parallel algorithm program is divided into three parts. The first part creates $M$ threads which are dived into Blm blocks, and the $m$th thread deals with the $m$th leaves with the four-path method. Each block has bm threads, and the fields in the same block are kept in the shared memory, see Fig. 6. The second part creates $N$ threads, and the $n$th thread deals with the first order field of the $n$th trunk. The third part creates $N*(N-1)$ threads which are divided into Bln blocks, and the threads are identified by $i$ and $n$. each thread calculates the second order field $\vec{E}^s_{nittg} + \vec{E}^s_{nitgt} + \vec{E}^s_{nigtt}$.

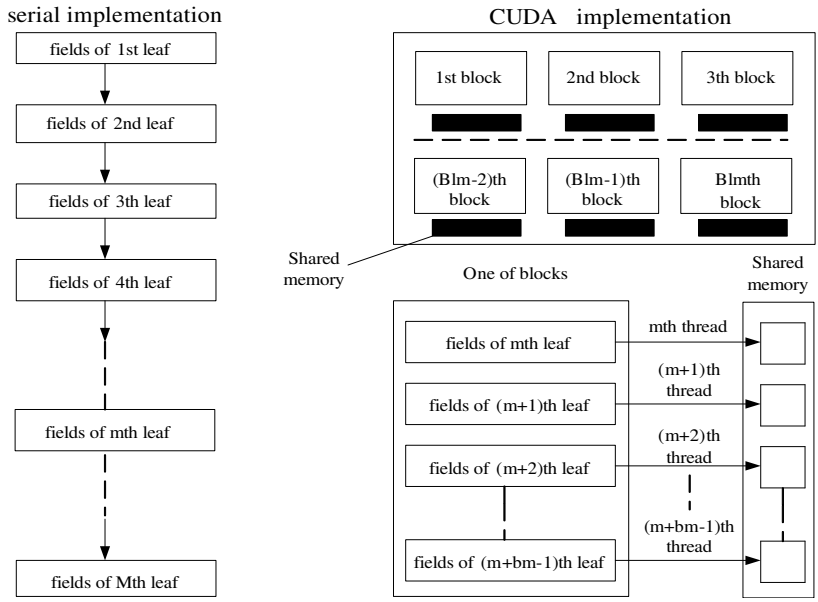


**Figure 6.** Process of calculating backscattering from crown-layer.

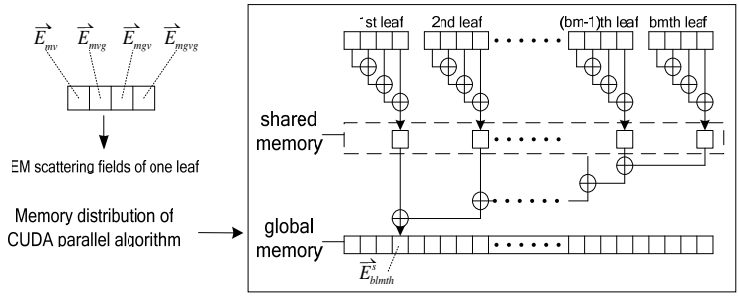


**Figure 7.** Memory distribution of the first part.

The fields in the same block are also added, shown in Fig. 7. By using the shared memory, the parallel program can reduce the requirement of GPU global memory which is need more time to read and write. For the random function is a serial process, the process of sampling the position and orientation of the $M$ leaves and $N$ trunks of the CUDA parallel algorithm is on the CPU. Due to the CUDA's ability of parallel computing, the CUDA-based method can calculate the EM scattering properties from the vegetation more quickly and reaches a speedup of 294 times with a GTX 460 GPU as a coprocessor. Thus, we can obviously improve the speed of calculating the EM scattering properties from a field in large scope.

We calculate the EM scattered field from a three-layer canopy with the parameters given by Tab. 1. Fig. 8 shows the total backscattering coefficient, the backscattering coefficient of crown-layer and the scattering coefficient of trunk-layer. The results obtained by the parallel algorithm fit well with those obtained by the serial algorithm. That indicates that the CUDA-based method is feasible and accurate enough to simulate the EM scattering properties of the vegetation.

Figures 9 and 10 show, respectively, the backscattering coefficient of the HH and VV polarization, with the trunk number density of $0.5/\mathrm{m}^3$ and $2/\mathrm{m}^3$ under the CUDA-based method. And the results are averaged values over 1000 iterations. The HH polarization backscattering coefficient of the three-layer canopy increases a little with the increase of the number density, shown in Fig. 9. However, the VV polarization backscattering coefficient drops more quickly with the incident angle, when the number density of trunks is $2/\mathrm{m}^3$. For the

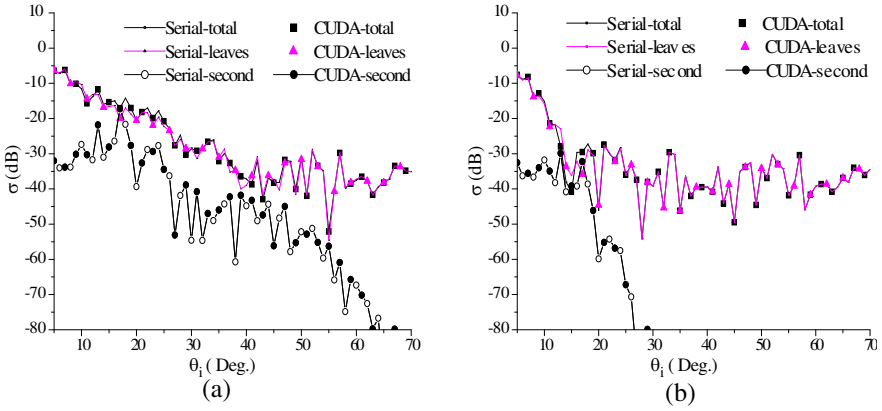


**Figure 8.** Results of backscattering coefficient of two methods (frequency = 3 GHz). (a) HH polarization, (b) VV polarization.

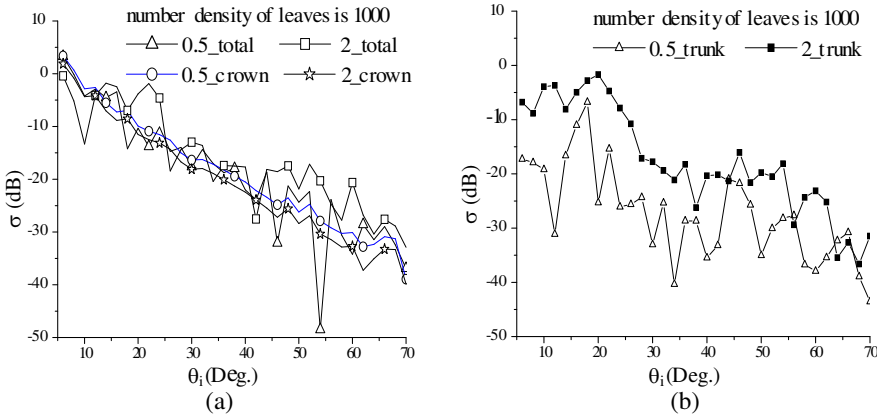


**Figure 9.** HH polarization ($r_g$ = 2 m and Frequency = 3 GHz). (a) Backscattering coefficient of total canopy and crown layer, (b) backscattering coefficient of trunk layer.

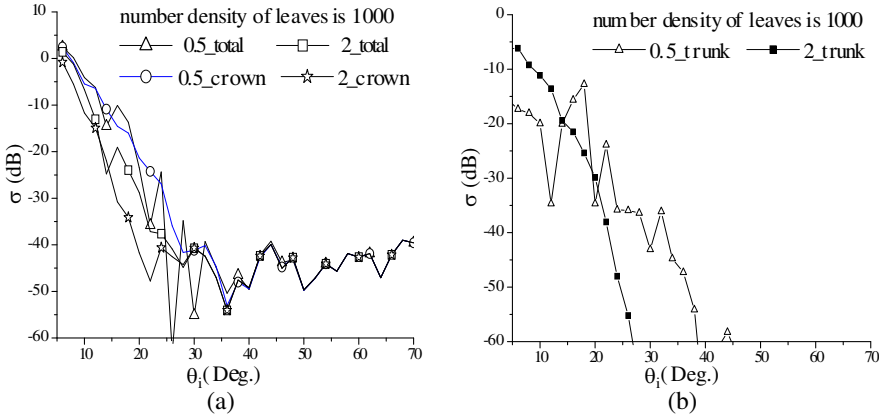


**Figure 10.** VV polarization ($r_g$ = 2 m and Frequency = 3 GHz). (a) Backscattering coefficient of total canopy and crown layer, (b) backscattering coefficient of trunk layer.

trunks are vertically placed on the ground, the absorption of the VV polarization is more obviously, when the number density of trunks gets larger, and the VV polarization coefficient drop more quickly. The VV polarization coefficient of the crown layer plays the main role when the incident angle becomes large, shown in Fig. 10.

Figure 11 shows the backscattering coefficient from a three-layer canopy of radius 20 meters. And the number densities of leaves and trunks are $1000/\mathrm{m}^3$ and $1/\mathrm{m}^2$, respectively. There are 376991 leaves

and 1256 trunks. The CUDA parallel program takes 2.76 minute to calculate the backscattering coefficient of the crow-layer and 40.23 minutes ms to calculate the backscattering of the trunk-layer. It is quite quick to calculate EM scattering properties of the vegetation of large scope.

The Tab. 2 and Fig. 12 show the time consumed by programs and the ration of calculating time of CUDA-based method to that of traditional method. The CUDA parallel algorithm calculates more quickly than the serial algorithm. The symbol $r_g$ is the radius of the ground. With other parameters unchanged, the efficiency of the CUDA-based method increases with the increase of the radius. The CUDA parallel program's ability in executing hundreds threads simultaneity on the GPU let it can deal with hundreds of targets at a time. Thus, it calculates faster than the traditional serial program. Furthermore, the CUDA parallel program has the ability to read and write memory for the threads while other threads are executing on

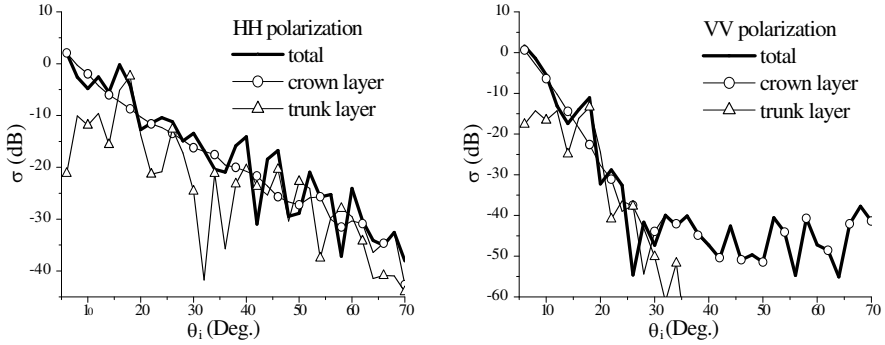


**Figure 11.** Backscattering coefficient from three-layer canopy of radius 20 meters (frequency = 3 GHz).

**Table 2.** Time (ms) consumed by programs and ratio of time (serial's/CUDA's).

| | Time(ms) consumed by programs | | | | Ratio of time | | | |
|---|---|---|---|---|---|---|---|---|
| | $r_g$ =1 | $r_g$ =2 | $r_g$ =3 | $r_g$ =4 | $r_g$ =1 | $r_g$ =2 | $r_g$ =3 | $r_g$ =4 |
| First part of serial's | 13235 | 51610 | 115891 | 206469 | 1.0 | 1.0 | 1.0 | 1.0 |
| First part of CUDA's | 547 | 1797 | 3828 | 6703 | 24.2 | 28.7 | 30.3 | 30.8 |
| Last part of serial's | 1812 | 43890 | 244672 | 786984 | 1.0 | 1.0 | 1.0 | 1.0 |
| Last parts of CUDA's | 1047 | 1094 | 1250 | 2672 | 1.7 | 40.1 | 195.7 | 294.5 |
| Total part of serial's | 15047 | 95500 | 360563 | 993453 | 1.0 | 1.0 | 1.0 | 1.0 |
| Total part of CUDA's | 1594 | 2891 | 5078 | 9375 | 9.4 | 33.0 | 71.0 | 106.0 |

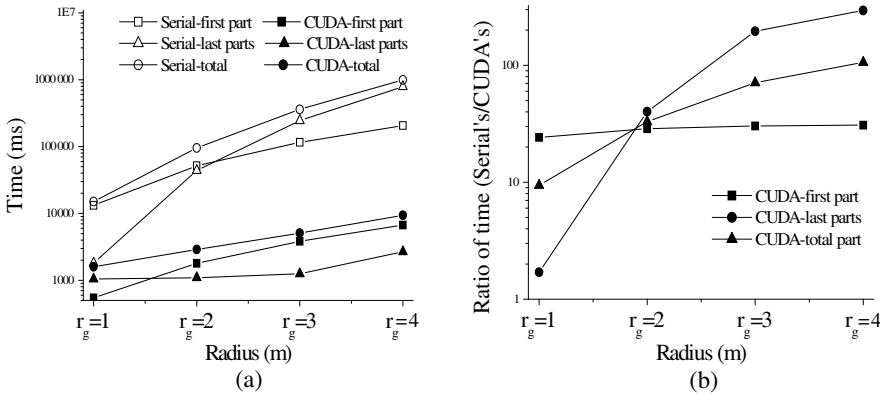


**Figure 12.** Comparison of serial program and CUDA parallel program. (a) Time (ms) consumed by programs, (b) ratio of time (serial's/CUDA's).

the Arithmetic Logic Units (ALU) in the GPU. This makes the CUDA parallel program performs more efficient when the number of scatterers gets larger. For the three-layer canopy, we get a highest speedup of 294 times. It is a quite quick to calculate the EM scattering problem of the vegetation. And the CUDA-based method is feasible to simulate the EM scattering properties of vegetation in large scope.

## 4. CONCLUSION

The CUDA-based method and its application to a Monte-Carlo simulated three-layer canopy model are discussed. It is accurate enough to calculate the EM scattering problem, and the results fit the measured data well. Due to its ability of parallel computing, it can help calculate the EM scattered fields from hundreds of targets at the same time with a speedup of several hundred times. Furthermore, when the number of scatterers gets large, the CUDA-based method performs more efficiently. It will be feasible to implement the simulation of the EM scattering from vegetation in large scope.

## ACKNOWLEDGMENT

The authors would like to thank the anonymous reviewers for their invaluable comments and suggestions, which lead to great improvement of our manuscript, and also thank the National Natural Science Foundation of China under Grant No. 60871070, the National Pre-research Foundation and the Foundation of the Science and Technology on Electromagnetic Scattering Laboratory to support this kind of research.

## REFERENCES


1. Levine, D., "The radar cross section of dielectric disks," *IEEE Trans. Antennas Propag.*, Vol. 32, No. 11, 6–12, 1984.
2. Gay-Fernandez, J. A., M. Garcia Sanchez, I. Cuinas, A. V. Alejos, J. G. Sanchez, and J. L. Miranda-Sierra, "Propagation analysis and deployment of a wireless sensor network in a forest," *Progress In Electromagnetics Research*, Vol. 106, 121–145, 2010.
3. Schiffer, R. and K. O. Thielheim, "Light scattering by dielectric needles and disks," *Appl. Phys.*, Vol. 50, No. 4, 2476–2483, 1979.
4. Bonafoni, S., F. Alimenti, G. Angelucci, and G. Tasselli, "Microwave radiometry imaging for forest fire detection: a simulation study," *Progress In Electromagnetics Research*, Vol. 112, 77–92, 2011.
5. Karam, M. A., A. K. Fung, and Y. M. M. Antar, "Electromagnetic wave scattering from some vegetation samples," *IEEE Trans. Geosci. Remote Sensing*, Vol. 26, No. 6, 799–808, 1988.
6. Meng, Y. S., Y. H. Lee, and B. C. Ng, "Experimental dynamical evolution of the brillouin precursor for broadband wireless communication through vegetation," *Progress In Electromagnetics Research*, Vol. 111, 291–309, 2011.
7. Du, Y., Y. Luo, W. Z. Yan, and J. A. Kong, "High angular resolution measurements of the monostatic backscattering coefficient of rice fields," *Journal of Electromagnetic Waves and Applications*, Vol. 23, No. 1, 1–10, 2009.
8. Du, Y., W.-Z. Yan, J.-C. Shi, Z. Li, and E.-X. Chen, "Electromagnetic scattering from a corn canopy at $L$ and $C$ Bands," *Progress In Electromagnetics Research*, Vol. 114, 33–49, 2011.
9. Singh, D., V. Srivastava, B. Pandey, and D. Bhimsaria, "Application of neural network with error correlation and time evolution for retrieval of soil moisture and other vegetation variables," *Progress In Electromagnetics Research B*, Vol. 15, 245–265, 2009.
10. Ulaby, F. T., K. Sarabandi, K. McDonald, et al., "Michigan microwave canopy scattering model (MIMICS)," *Int. J. Remote Sensing*, Vol. 11, No. 7, 1223–1253, 1990.
11. Johnson, J. T., "A study of the four-path model for scattering from an object above a half space surface," *Microwave and Optical Technology Letters*, Vol. 30, No. 2, 130–134, 2001.
12. Koay, J. Y., H. T. Ewe, and H. T. Chuah, "Effects of fresnel corrections in the scattered field of general ellipsoids," *Progress*

*In Electromagnetics Research Proceedings*, Vol. 3, No. 2, 213–214, March 26–30, 2007.

13. Acquista, C., "Light scattering by tenuous particles: a generalization of the Rayleigh-Gans_Rocard approach," *Appl. Opt.*, Vol. 15, No. 11, 2932–2936, 1976.
14. Sarabandi, K., P. F. Polatin, and F. T. Ulaby, "Monte carlo simulation of scattering from a layer of vertical cylinders," *IEEE Trans. on Antennas and Propagation*, Vol. 41, No. 4, 465–473, 1993.
15. Garland, M., S. Le Grand, J. Nickolls, et al., "Parallel computing experiences with CUDA," *IEEE Micro.*, Vol. 28, No. 4, 13–27, 2008.
16. Hwu, W. M., C. Rodrigues, S. Ryoo, and J. Stratton, "Compute unified device architecture application suitability," *Computing in Science & Engineering*, Vol. 11, No. 3, 16–26, 2009.
17. Tao, Y. B., H. Lin, and H. J. Bao, "From CPU to GPU: GPU-based electromagnetic computing (GPUECO)," *Progress In Electromagnetics Research*, Vol. 81, 1–19, 2008.
18. Zainud-Deen, S. H., E. El-Deen, M. S. Ibrahim, K. H. Awadalla, and A. Z. Botros, "Electromagnetic scattering using GPU-based finite difference frequency domain method," *Progress In Electromagnetics Research B*, Vol. 16, 351–369, 2009.
19. Jiang, W. Q., M. Zhang, and Y. Wang, "CUDA-based radiative transfer method with its application to the EM scattering from a two-layer canopy model," *Journal of Electromagnetic Waves and Applications*, Vol. 24, No. 17–18, 2509–2521, 2010.
20. Donno, D. D., A. Esposito, L. Tarricone, and L. Catarinucci, "Introduction to GPU computing and CUDA programming: a case study on FDTD," *IEEE Antennas Propag. Mag.*, Vol. 52, No. 3, 117–122, 2010.
21. Gao, P. C., Y. B. Tao, and H. Lin, "Fast RCS prediction using multiresolution shooting and bouncing ray method on the GPU," *Progress In Electromagnetics Research*, Vol. 107, 187–202, 2010.
22. Zunoubi, M. R., J. Payne, and W. P. Roach, "CUDA implementation of TEz-FDTD solution of Maxwell's equations in dispersive media," *IEEE Antennas Wireless Propag. Lett.*, Vol. 9, 756–759, 2010.
23. Xu, K., Z. H. Fan, D. Z. Ding, and R. S. Chen, "GPU accelerated unconditionally stable crank-nicolson FDTD method for the analysis of three-dimensional microwave circuits," *Progress In Electromagnetics Research*, Vol. 102, 381–395, 2010.

24. Tao, Y., H. Lin, and H. Bao, "GPU-based shooting and bouncing ray method for fast RCS prediction," *IEEE Trans. Antennas Propag.*, Vol. 58, No. 2, 494–502, 2010.
25. Zhang, M., Y. X. Song, et al., "Simulation of low-grazing scattering properties of vegetation," *Chin. Phys. Lett.*, Vol. 20, No. 4, 502–505, 2003.
26. Du, Y., Y. Luo, W. Z. Yan, and J. A. Kong, "An electromagnetic scattering model for soybean canopy," *Progress In Electromagnetics Research*, Vol. 79, 209–223, 2008.
27. Karam, M. A. and A. K. Fung, "Leaf-shape effects in electromagnetic wave scattering from vegetation," *IEEE Trans. Geosci. Remote Sens.*, Vol. 27, No. 6, 687–697, 1989.
28. Matthaeis, P. D. and R. H. Lang, "Microwave scattering models for cylindrical vegetation components," *Progress In Electromagnetics Research*, Vol. 55, 307–333, 2005.
29. Toan, T. L., F. Ribbes, L. F. Wang, N. Floury, K. H. Ding, J. A. Kong, M. Fujita, and T. Kurosu, "Rice crop mapping and monitoring using ERS-1 data based on experiment and modeling results," *IEEE Trans. Geosci. Remote Sens.*, Vol. 35, No. 1, 41–56, 1997.
30. Yueh, S. H., J. A. Kong, J. K. Jao, R. T. Shin, and T. L. Toan, "Branching model for vegetatation," *IEEE Trans. Geosci. Remote Sens.*, Vol. 30, No. 2, 390–402, 1992.
31. Wang, L., J. A. Kong, K. H. Ding, T. L. Toan, F. R. Baillarin, and N. Floury, "Electromagnetic scattering model for rice canopy based on monte carlo simulation," *Progress In Electromagnetics Research*, Vol. 52, 153–171, 2005.
32. Lang, R. H., "Electromagnetic backscattering from a sparse distribution of lossy dielectric scatterers," *Radio Science*, Vol. 16, No. 1, 15–30, 1981.
33. Au, W. C., L. Tsang, R. T. Shin, and J. A. Kong, "Collective scattering and absorption effects in microwave interaction with vegetation canopy," *Progress In Electromagnetics Research*, Vol. 14, 181–231, 1996.
34. Sarabandi, K. and P. F. Polatin, "Electromagnetic scattering from two adjacent objects," *IEEE Trans. Antennas Propag.*, Vol. 42, No. 4, 510–517, 1994.
35. Ruck, G. T., D. E. Barrick, W. D. Stuart, and C. K. Krichbaum, *Radar Cross Section Handbook*, Plenum Press, New York and London, 1970.